Proceeding Paper

Multilevel Phase Switch Generation in Alkali Vapors [†]

Abu Mohamed Alhasan [1,2,*,‡] (ID) **and Salah Abdulrhmann** [1,3] (ID)

1   Department of Physics, Faculty of Science, Assiut University, Assiut 71516, Egypt
2   Bağlar Mahallesi, 31500 Ryhanlı, Hatay, Turkey
3   Department of Physics, Faculty of Science, Jazan University, P.O. Box 114, Jazan 45142, Saudi Arabia
*   Correspondence: am.alhasan.sq@gmail.com
†   Presented at the 3rd International Electronic Conference on Applied Sciences, 1–15 December 2022;
     Available online: https://asec2022.sciforum.net/.
‡   Retired.

Abstract: We attempt to demonstrate optical phase switches in a typical light storage experiment. We computed propagation dynamics of light pulses in sodium-23, rubidium-87, and potassium-39 vapors. These vapors have the same tensorial sets of the density matrix with a nuclear spin $I = 3/2$. The energy scheme is known as the double-Λ system. We considered an excitation mechanism in which one of two Λ systems was excited by two-color pulses, probe, and drive, following the standard electromagnetically induced transparency configuration. The probe channel contains delayed two pulses after the first probe pulse. Gain is generated through the drive channel and is exposed during propagation. We further investigated the spatiotemporal phase variations in the pulses and found discrete phase distribution for different vapors. The spatiotemporal evolution of the irreducible tensorial sets defines structural differential equations. Additionally, it is particularly suitable for parallel processing. We hope our study finds an application in comparison to alkali vapor magnetometry.

Keywords: alkali vapor; hyperfine structure; Gaussian train propagation; phase sensitivity; Maxwell–Bloch equations

1. Introduction

Recently, light storage and its retrieval have become some of the fundamental aspects of applied quantum technology (AQT) [1,2]. In the context of electromagnetically induced transparency (EIT) [3,4], light storage has been verified experimentally in gases [3] and solids [5]. In rubidium vapors, Buser et al. showed the storage of a single photon and its retrieval [1]. Additionally, Korzeczek et al. proposed a technique for using a magnetic field to control the deflection of the restored pulse [6]. Moreover, Xu et al. studied a double Λ system that interacted with dual laser fields and discussed the influence of a magnetic field on the relative phase of the radiation fields [7]. The double system becomes phase-insensitive as it is reduced to the single Λ system. Once turning on the magnetic field, the system transforms into a phase-sensitive one. In this paper, we are particularly interested in the phase generated by the hyperfine splitting structure in alkali vapors and the phase owing to pulse shaping during propagation. We assume that the hyperfine structure is resolved, which is an adequate assumption for cooled atoms [8].

2. The Atomic System

The energy-level diagram of alkali metal atoms ^{23}Na, ^{87}Rb, and ^{39}K is shown in Figure 1. We consider the transitions $n\,^2S_{1/2} - n\,^2P_{1/2}$, where $n = 3$, 5, and 4, for sodium, rubidium and potassium vapors, respectively. The kets $|1\rangle = |n\,^2S_{1/2}, F = 1\rangle$, $|2\rangle = |n\,^2S_{1/2}, F = 2\rangle$, and $|3\rangle = |n\,^2P_{1/2}, F = 1\rangle$, $|4\rangle = |n\,^2P_{1/2}, F = 2\rangle$ refer to the lower and upper hyperfine states, respectively. The quantum number F stands for the total angular momentum. The

probe and drive fields are detuned by Δ_p and Δ_r from the transitions $|1\rangle \leftrightarrow |3\rangle$ and $|2\rangle \leftrightarrow |3\rangle$, respectively. For experimental atomic data on alkali metal vapors, we refer to [9–12]. The fields with Rabi frequencies Ω_p and Ω_r connect the optical transitions $|1\rangle \rightarrow |3\rangle$, $|4\rangle$ and $|2\rangle \rightarrow |3\rangle$, $|4\rangle$, respectively.
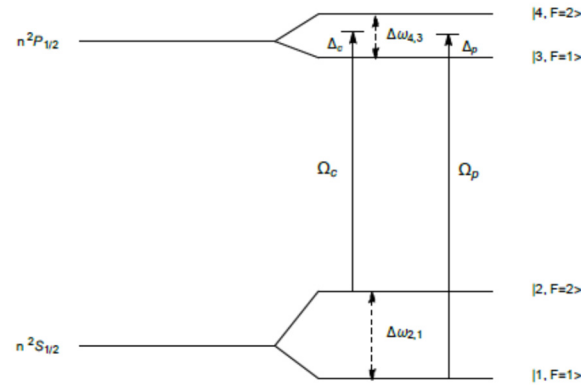
Figure 1. The atomic hyperfine structure of an alkali metal atom with nuclear spin $I = 3/2$. It corresponds to transitions $3\,^2S_{1/2} - 3\,^2P_{1/2}$, $5\,^2S_{1/2} - 5\,^2P_{1/2}$, and $4\,^2S_{1/2} - 4\,^2P_{1/2}$ for ^{23}Na, ^{87}Rb, and ^{39}K vapors, respectively. The one-photon detuning for the probe and drive fields are denoted by Δ_p and Δ_r, respectively. The two-photon detuning $\Delta\omega_{2,1}$ and $\Delta\omega_{4,3}$ denote lower and upper hyperfine splitting, respectively.

The time evolution of the reduced density matrix $\rho_s(t)$ is given by the first-order Liouville–von Neumann differential equation

$$-i\frac{\partial\rho_s(t)}{\partial t} = \hat{\mathcal{L}}_t\rho_s(t), \; \hbar = 1, \tag{1}$$

where $\hat{\mathcal{L}}_t$ stands for the Liouvillian super-operator in the Liouville space [13–15]. The formalism of Fiutak and Van Kranendonk has been extended for two-level atoms with a fine structure [13] to the case of multilevel atoms with hyperfine structures [16,17].

Let (z, t) represent space–time coordinates in the laboratory frame, and c is the light speed. The dimensionless retarded time is expressed as $\tau = \gamma(t - z/c)$ in a frame moving with the pulse. Additionally, γ is the spontaneous decay rate of the excited atomic-state $P_{1/2}$. Furthermore, $\zeta = \alpha'(z + ct)$ gives the dimensionless space variable, and α' is the absorption coefficient. The atom field coupling is defined from $v = dE/2\sqrt{3}$, where d is the dipole moment of the optical transition and E is the electric field amplitude. The Rabi frequency is related to atom field coupling through the relation $\Omega = \sqrt{8}v$. The relative atom–field coupling becomes $\mathsf{v} = v/\gamma$.

In the following, we describe the irreducible tensorial set (ITS) components associated with a nuclear spin $I = 3/2$. Recently, the mathematical formalism of ITS for atoms and molecules has been reviewed [18]. We have 28 density matrix components as $\rho_{\alpha\beta}^{(Fm)}$ [16]. The indices α and β take values from 1 to 4, while F is the tensor rank, representing the total angular momentum. Additionally, m is the magnetic quantum number. Throughout, we will adopt convention $\rho_{\alpha,\beta}^{(Fm)}$ for the density matrix, and the notation $\rho_{\alpha\beta}^{(Fm)}$ denotes its counterpart on the product space [16].

Figure 2 shows the pulse profiles for $\Omega_p(\tau)$ and $\Omega_r(\tau)$ fields for different alkali vapors. At the entrance point $\zeta = 0$, the pulses are truncated-Gaussian in shape and characterized by the same amplitude and different widths. The drive pulse is a single pulse where the probe consists of a train of Gaussian pulses. In sodium vapor, the pulses do not exactly overlap in time.
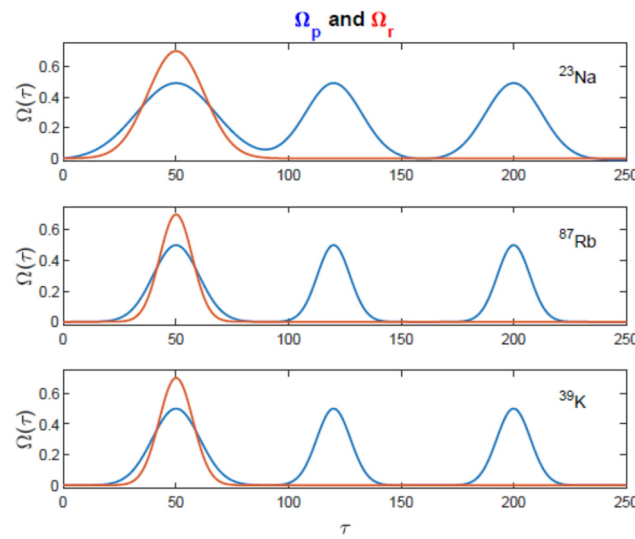
Figure 2. Pulse profiles for $\Omega_p(\tau)$ and $\Omega_r(\tau)$ fields at the entrance point $\zeta = 0$ for different alkali vapors. Time, as well as Rabi frequencies associated with the probe and drive channels, are presented in relative units.

The first probe pulse in the train is wider than the drive pulse. Let w stand for the width of the pulse. Additionally, γ is the spontaneous decay rate of the $n\ {}^2P_{1/2}$ state. Thus, we have the triple $\{\{\gamma_{Na}, w_{Na}\}, \{\gamma_{Rb}, w_{Rb}\}, \{\gamma_K, w_K\}\}$ for the alkali vapors. The width of the pulse in potassium vapor is diminished by $w_K = (\gamma_K/\gamma_{Na})w_{Na}$. The shrinking in the widths of rubidium and potassium leads to well-resolved pulses without overlap. For the sodium case, this is not true, especially for the first and second pulses. It overlaps at the far wings. In our calculations, we have kept the amplitude v_0 to be the same, according to $\frac{v_0^{Na}}{\gamma_{Na}} = \frac{v_0^{Rb}}{\gamma_{Rb}} = \frac{v_0^K}{\gamma_K}$. The pulses are degenerate with respect to the field amplitudes. The degeneracy can be resolved with respect to the intensity I as $\left(\frac{\Omega}{\gamma}\right)^2 = \frac{I}{I_s}$, where I_s is the saturation intensity.

The time evolution of the dressed atom is determined by the Liouville–von Neumann-type equation. We present it in the matrix form as

$$\frac{\partial \rho(t)}{\partial t} = L\left(t, \gamma, \Delta\omega_{4,3}, \Delta\omega_{2,1}, \Delta_p, \Delta_r, v_p, v_r, \gamma_{coll}^{(k)}\right)\rho(t), \tag{2}$$

where $\gamma_{coll}^{(k)}$ represents the collisional relaxation rates of rank k. Equation (2) forms the Bloch equation for the density matrix [16]. There are three Bloch sets of equations corresponding to different vapors under consideration. Additionally, there are three sets of reduced field equations which describe the space evolution. The reduced Maxwell field equations in the slowly varying approximation can be separated as

$$\frac{\partial v_p(z,t)}{\partial z} = \frac{\alpha'_p}{\sqrt{6}}\left[\rho_{3,1}^{(10)}(z,t) - \sqrt{5}\rho_{4,1}^{(10)}(z,t)\right],$$
$$\tag{3}$$
$$\frac{\partial v_r(z,t)}{\partial z} = \frac{\alpha'_r}{\sqrt{2}}\left[\rho_{3,2}^{(10)}(z,t) - \rho_{4,2}^{(10)}(z,t)\right],$$

where α_p and α_r denote the absorption coefficients of the probe and drive fields, respectively. Initially, we assume that the atoms occupy the first hyperfine level, i.e., $\sqrt{3}\rho_{1,1}^{(00)} = 1$, which is beyond the so-called phaseonium medium introduced by Scully [19]. For such a medium, Clader and Eberly have obtained interesting explicit analytical results for two-color propagation in a single Λ medium for ultrashort pulse propagation [20]. In this paper, the pulse arrangements are beyond the conventional electromagnetically induced

transparency setup. It is more convenient to make use of relative units. The reduced Maxwell field equations can be written as

$$\frac{\partial}{\partial \varsigma} v_p(\varsigma, \tau) = \sqrt{6^{-1}} \left[\rho_{3,1}^{(10)}(\varsigma, \tau) - \sqrt{5} \rho_{4,1}^{(10)}(\varsigma, \tau) \right],$$

$$\frac{\partial}{\partial \varsigma} v_r(\varsigma, \tau) = \sqrt{2^{-1}} \left[\rho_{3,2}^{(10)}(\varsigma, \tau) - \rho_{4,2}^{(10)}(\varsigma, \tau) \right], \tag{4}$$

$$\frac{\partial}{\partial \tau} \rho(\tau) = \frac{1}{\gamma} L \left(\tau, \gamma, \Delta\omega_{4,3}, \Delta\omega_{2,1}, \Delta_p, \Delta_r, v_p, v_r, \gamma_{coll}^{(k)} \right) \rho(t),$$

Initially, we assume real-valued Rabi frequencies, where phases of the fields and the atomic dipoles are absent.

3. Numerical Results

The Rabi frequency associated with the probe and drive fields is expressed as $\Omega_p = 2\sqrt{3}v_p$ and $\Omega_r = 2\sqrt{3}v_r$ in relative units, respectively. Figure 2 shows three time sections for the interaction time. The duration $T_1 = \{\tau \mid \tau \in [0\ 85]\}$ is accompanied by an extension of the probe pulse beyond the drive pulse. The duration $T_2 = \{\tau \mid \tau \in (85\ 170]\}$ represents the second probe pulse in the pulse train and belongs to the first generated pulse in the drive channel. The time T_2 presents separate pulses in the probe channel for rubidium and potassium vapors. The last time section, $T_3 = \{\tau \mid \tau \in (170\ 250]\}$, represents the time of the second generated pulse.

Figure 3 illustrates phase patterns resulting from the drive channel as a function of time for different prolonged distances inside a sodium gas medium. Probe and drive fields are resonantly coupled to the excited hyperfine state $|3, F = 1\rangle$. Phase patterns are presented through weak criteria, in which the phases are mainly produced by the second (upper) and perturbing Λ subsystem. Beyond that, at the injection point, $\zeta = 0$, the drive pulse indicates phase switching from zero to π, with a starting time of $\tau = 100$ and corresponding to the T_2 interval. Through such a period, the pulse envelope profile undergoes interference between the far end of the first pulse and the leading edge or the front of the second pulse in the train. Notably, the phase remains zero for times within the conventional EIT, T_1 section. For long time sections, such as T_2 and T_3, we have noticed the generation of drive pulses. The generated pulses in the drive channel propagate across the medium with different phase patterns.
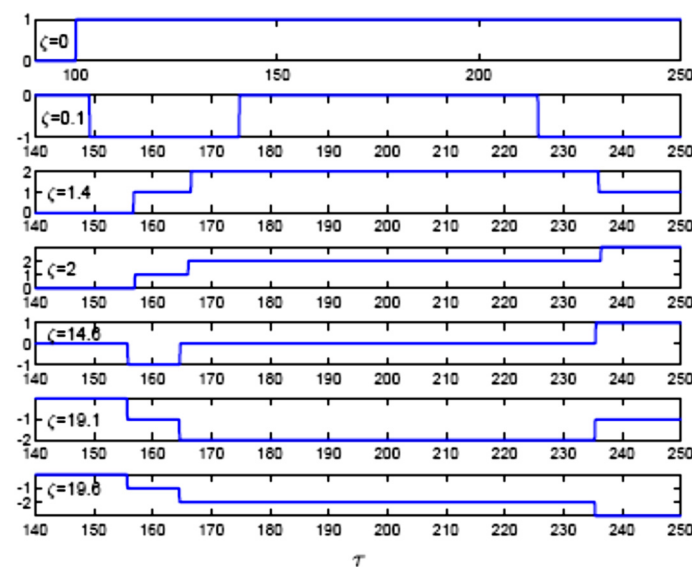

Figure 3. Temporal phase trajectories are associated with the drive channel for different prolonged distances inside sodium vapor. The phase is presented in π units.

As a result of the interplay between phase generation and time sections, this leads to phase production, which is due to the interference between the rising and falling edges of the neighborhood pulses and resulting from the detuning of upper hyperfine splitting. Moreover, the width of the generated $\pm\pi$ switch is not regular for different sequences through propagation.

We turn to the relative phase of the generated pulses in the drive channels concerning the corresponding probe pulses. The relative phase is defined as

$$\Phi_{rp}(\zeta, \tau) = \frac{1}{\pi}\{\Phi_r(\zeta, \tau) - \Phi_p(\zeta, \tau)\} \tag{5}$$

Figure 4 presents the relative phase at the same space points as located in Figure 3. There are seven discrete phase distributions for alkali vapors. The first phase distribution, $S_1^{\{Na,Rb,K\}}$, denotes the relative phase at the injection point of pulses. The relative phase maintains the π value within the interaction period T_1, that is mainly the duration of the first pulses of the probe and drive pulses. At later times, interference becomes significant. This results in phase switching to 0π and π again. At different prolonged distances inside the medium, the relative phases S_2 to S_7 act as a compensation between the phases due to complex pulse shaping reforms and the detuning of the upper hyperfine splitting. The $\pm\pi$-switches are distributed among different phase trajectories. The phase distribution, S_1, in Figure 4, indicates deviations in phases regarding distinct pulse shaping effects. For long time, there is an enhancement of phase switches produced in $S_2^{\{K,Rb\}}$, $S_3^{\{K,Rb\}}$, and $S_4^{\{K,Rb\}}$ for rubidium and potassium vapors. Thus, one can distinguish such differences between rubidium and potassium as a group and sodium. The relative phase switches in rubidium and potassium stabilize at higher values than for sodium, for long distances. The phase switch stabilizes at 0π or π for sodium vapors, whereas for potassium and rubidium, we have the discrete distribution as $S_7^{\{K,Rb\}} = \{0\pi, \pi, \pi, 2\pi, 3\pi, 2\pi\}$. Accordingly, we have two limits for the relative phase in sodium. It is either π or 0π at T_3. However, in $S_7^{\{K,Rb\}}$, we have only the values 2π and 3π. The atomic spontaneous decay rates for the potassium and rubidium are close. Sodium vapors have the highest relaxation rate, and the upper hyperfine splitting of rubidium is approximately 15 times bigger than that of potassium. Therefore, we can conclude that our results depend strongly on the spontaneous relaxation rate rather than the upper hyperfine splitting.
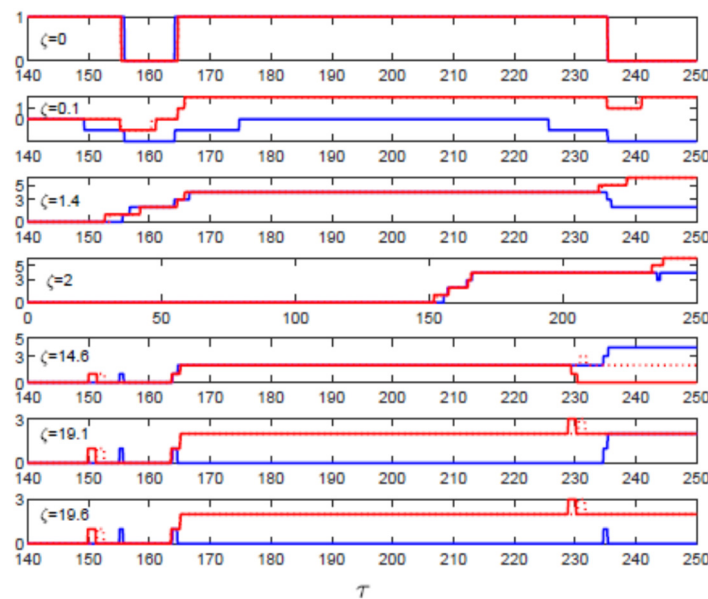
Figure 4. The relative phase of the drive pulses at different distances is depicted. The relative phase is presented in π units. The shape of the initial pulses is as presented in Figure 2.

4. Discussion

We have explored time-dependent discrete phase distributions in alkali atom vapors concerning hyperfine structures with a nuclear spin $I = 3/2$. We provided an incomplete scheme for the light storage-like experiments in which, for relativity short times, probe and writing drive pulses are the exciting pulses with an absence of the read pulse and two pulses added in the probe channel. The Stokes fields are generated in the drive channels toward the minimum uncertainty products. The fields were real initially, and the system was phase-sensitive. We have achieved this through the manipulation of wing–wing mutual interaction. As a result, we have shown digital phase modulations with a discrete sequence of values defined over different interval widths. The digital signals are developed as rectangular π-pulses with a constant phase, except for step changes at interval boundaries without ramping, i.e., the rectangular transitions are not smoothed. For relatively moderate fields, the phase levels approach π, 0π for sodium and 3π, 2π for rubidium and potassium.

References

1. Buser, G.; Mottola, R.; Cotting, B.; Wolters, J.; Treutlein, P. Single-Photon storage in a Ground-State vapor cell quantum memory. *PRX Quantum* **2022**, *3*, 020349-1–020349-10. [CrossRef]
2. Esguerra, L.; Mesner, L.; Robertson, E.; Ewald, N.V.; Gündoğan, M.; Wolters, J. Optimization and readout-noise analysis of a hot vapor EIT memory on the Cs D1 line. *arXiv* **2022**, arXiv:2203.06151.
3. Phillips, D.F.; Fleischhauer, A.; Mair, A.; Walsworth, R.L.; Lukin, M.D. Storage of light in atomic vapor. *Phys. Rev. Lett.* **2001**, *86*, 783. [CrossRef] [PubMed]
4. Liu, C.; Dutton, Z.; Behroozi, C.H.; Hau, L.V. Observation of coherent optical information storage in an atomic medium using halted light pulses. *Nat. Lond.* **2001**, *409*, 490–493. [CrossRef] [PubMed]
5. Riedmatten, H.D.; Afzelius, M. Quantum light storage in solid state atomic ensembles. In *Engineering the Atom-Photon Interaction*; Predojevic, A., Mitchell, M.W., Eds.; Springer: Cham, Switzerland, 2015; pp. 241–273.
6. Korzeczek, M.C.; Braun, D. Quantum router: Storing and redirecting light at the photon level. *Phys. Rev. A* **2021**, *104*, 063714. [CrossRef]
7. Xu, X.W.; Shen, S.; Xiao, Y.H. Tuning the phase sensitivity of a double-Λ system with a static magnetic field. *Opt. Exp.* **2013**, *21*, 11705–11714. [CrossRef] [PubMed]
8. Zhao, R.; Dudin, Y.O.; Jenkins, S.D.; Campbell, C.J.; Matsukevich, D.N.; Kennedy, T.A.B.; Kuzmich, A. Long-lived quantum memory. *Nat. Phys. Lett.* **2009**, *5*, 100. [CrossRef]
9. Arimondo, E.; Inguscio, M.; Violino, P. Experimental determinations of the hyperfine structure in the alkali atoms. *Rev. Mod. Phys.* **1977**, *49*, 31–75. [CrossRef]
10. van Wijngaarden, W.A.; Li, J. Measurement of hyperfine structure of sodium 3P1/2,3/2 states using optical spectroscopy. *Z. Phys. D* **1994**, *32*, 67–71. [CrossRef]
11. Rubidium 87 D Line Data. Version 2.2.2. Available online: http://steck.us/alkalidata (accessed on 9 July 2021).
12. Tiecke, T.G. Properties of potassium. Ph.D. Thesis, University of Amsterdam, Amsterdam, The Netherlands, 2010.
13. Fiutak, J.; van Kranendonk, J. The effect of collisions on resonance fluorescence and Rayleigh scattering at high intensities. *J. Phys. B At. Mol. Phys.* **1980**, *13*, 2869–2884. [CrossRef]
14. Dalton, B.J. Liouville space theory of sequential quantum processes. I. General theory. *J. Phys. A Math. Gen.* **1982**, *15*, 2157. [CrossRef]
15. Barnett, S.M.; Dalton, B.J. Liouville space description of thermofields and their generalizations. *J. Phys. A Math. Gen.* **1987**, *20*, 411. [CrossRef]

16. Alhasan, A.M. Entropy Associated with information storage and its retrieval. *Entropy* **2015**, *17*, 5920–5937. [CrossRef]
17. Alhasan, A.M. Density matrix description of fast and slow light propagation in Sodium vapor. *Open Syst. Inf. Dyn.* **2009**, *16*, 103–125. [CrossRef]
18. Methane Symmetry Operations-Irreducible Tensorial Sets. Available online: https://www.nist.gov/pml/methane-symmetry-operations/methane-symmetry-operations-irreducible-tensorial-sets (accessed on 2 June 2021).
19. Scully, M.O. From lasers and masers to phaseonium and phasers. *Phys. Rep.* **1992**, *219*, 191–201. [CrossRef]
20. Clader, B.D.; Eberly, J.H. Two-Pulse propagation in a partially phase-coherent medium. *Phys. Rev. A* **2008**, *78*, 03303. [CrossRef]